Supporting information

Regulating cation-solvent interactions in PVDF-based solid-state electrolytes for advanced Li metal batteries

Zhian Zhang[a], Meng Ye[a], Jianhua Chen[a], Xiaopeng Fu[a], Xunzhu Zhou[b], Limin Zheng[a], Liqing He[c], Zhenguo Wu[a], Amit Kumar[d], Lin Li*[b], Fang Wan*[a], and Xiaodong Guo[a]

Experimental Section

Preparation of PVDF-based electrolytes. Both lithium salt and zinc salt were dried at 80 °C for 24 h before use to remove water. The solution casting method was used to prepare different PVDF-based electrolytes. To prepare the PVDF-LiTFSI-LLZTO electrolyte (PLL), 1.08 g PVDF powders, 0.972 g LiTFSI, and 0.12 g LLZTO, were dissolved in 12 g DMF solvent and stirred at room temperature for 10 h. Furthermore, the solution was ball-milled with a speed of 500 rpm for 1 h in a stainless-steel jar to obtain a homogeneous solution. It should be noted that the main function of a small amount of LLZTO is to improve the film formation of PVDF-based electrolytes. The PVDF-LiTFSI-LLZTO-$Zn(TFSI)_2$ electrolyte (PLLZ) was prepared with the same procedure except that an additional 0.324 g $Zn(TFSI)_2$. The process for preparing PVDF-LLZTO-$Zn(TFSI)_2$ electrolyte (PLZ) is the same as that for preparing the PLLZ electrolyte but without adding LiTFSI. After that, the mixture was coated on a glass plate with a scraper. Finally, different PVDF-based electrolytes were further dried at 80 °C for 20 h in a vacuum oven.

Materials characterizations. To examine the chemical structure of obtained samples, Fourier-transform infrared Spectroscopy (FT-IR) was performed on Thermo Fisher Scientific Nicolet iS20 in the wavenumber range of 4000-400 cm^{-1}. The crystal structure information was characterized by X-ray diffractometer with Cu Kα radiation (XRD, PW3701, λ = 0.15418 nm). The chemical composition of the samples was analyzed by X-ray photoelectron spectroscopy (XPS) using Al Kα radiation (Thermo Scientific K-Alpha). ^{7}Li NMR experiments were measured on Bruker Avance Neo 400WB NMR spectrometer with a frequency of 400 MHz at ambient temperature. The Raman spectra were recorded by a Raman Spectrophotometer over the frequency range of 100-3200 cm^{-1} using a 532 nm excited laser at room temperature. The thermogravimetric analysis (TG) was carried out with nitrogen flowing over the samples on HITACHI STA200 at a heating rate of 5 °C min^{-1}. The morphology of the electrolyte membrane and Li anode were observed by scanning electron microscopy (SEM, ZEISS). A 3D optical profilometer (Sneox, Sensofar) was employed to scan the surface of samples, and the SensoScan software was used to analyze images.

Theoretical calculations. The interaction between Li^+ and DMF, and the effect of Zn^{2+} on the adsorption were studied by Materials Studio (MS). To further explore the ion transport mechanism in PVDF-DMF/LiTFSI electrolytes with/without the presence of $Zn(TFSI)_2$, Forcite method simulations were performed.[1,2] The electrochemical stability of different ions competitive adsorptions were studied by First-principle calculations using the DMol3 module and B3LYP.[3,4] The TS custom method was chosen for DFT-D. The convergence tolerance of the (a) maximum energy was 2×10^{-5} Ha, (b) maximum force was 0.004 Ha/Å and (c) maximum displacement was 0.005 Å. The COMPASSII was chosen as forcitefield. The unmodified composition molecules group was consisted by 13 LiTFSI, 65 PVDF and 15 DMF molecules. The modified composition molecules group was conducted by 13 LiTFSI, 2 $Zn(TFSI)_2$, 65 PVDF and 17 DMF molecules respectively. Each molecules group was optimized before explore the electronic properties.

Preparation of cathode. $LiFePO_4$ (LFP), which was from Canrd, was mixed with Super P and PVDF at a weight ratio of 8:1:1. After that, a moderate dose of N-1-methyl-2-pyrolidone (99.5 %, Sigma) and above mixture were added to the jar and ball milled for one hour to form homogeneous cathode slurry. The obtained slurry was then coated onto aluminum foil, followed by drying in a vacuum oven at 120 °C for 24 h.

Electrochemical measurements. The ionic conductivity of the electrolytes was confirmed by electrochemical impedance spectroscopy using the CHI660E system (LAND, China) from 30 to 80 °C. The electrolyte was sandwiched between two 15.8 mm diameter stainless-steel plates, while the frequency range was 10^{-1}-10^{-6} Hz with an amplitude of 5 mV.

The ionic conductivity was calculated using the following equation:

$$\sigma = L/RS$$

where L is the thickness of electrolytes, R is the bulk resistance, and S is the contact area between the electrolyte and blocking electrodes.

The active energy of ionic conducting was calculated by Arrhenius equation:

$$\sigma(T) \ = \ Aexp\,(-Ea/RT)$$

where σ is the ionic conductivity, A is pre-exponential constant, R is Boltzmann constant, Ea is active energy, and T is testing temperature.

The Li^+ transference number was verified by combining alternate-current impendence and direct-current polarization, according to the following equation:

$$t_{Li^+} = [I_s(\Delta V - I_0R_0)]/[I_0(\Delta V - I_sR_s)]$$

where I_0 and I_s are the initial and steady currents, respectively. R_0 and R_s represent the initial and steady interfacial resistance, respectively. ΔV is the polarization voltage (20 mV).

The electrochemical performance was tested by CR2025-type coin cells on a cell testing system (BTS). The coin cells were tested at room temperature with a voltage range of 2.7-3.9 V. Symmetric Li||Li cells were assembled by sandwiching the electrolyte between two Li anodes. All cells were assembled in the glovebox with O_2 and H_2O content below 0.1 ppm.

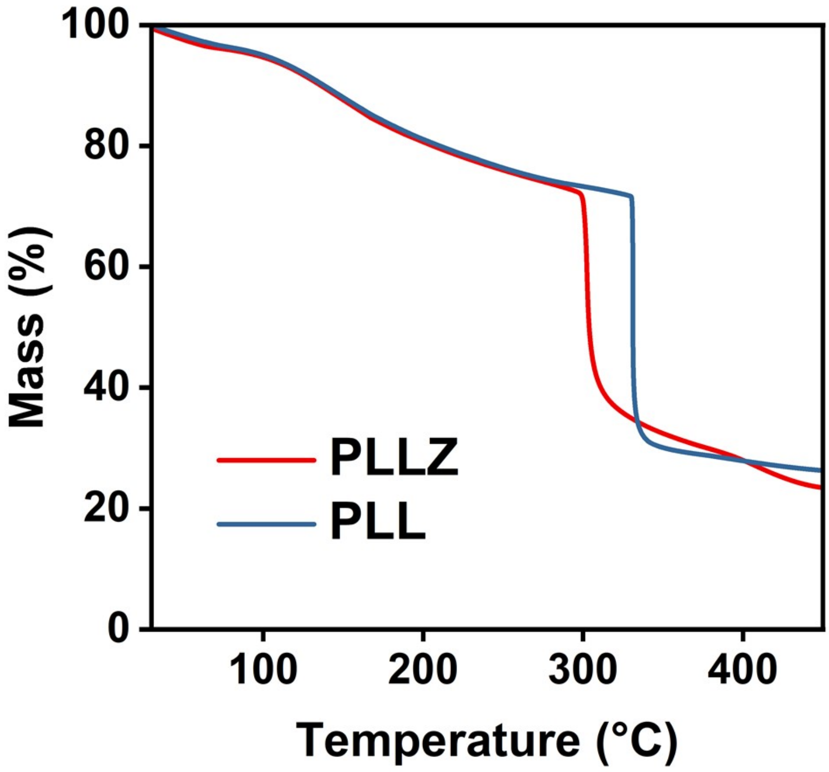

Figure S1. The thermal gravimetric analysis curves of PLL and PLLZ electrolytes.

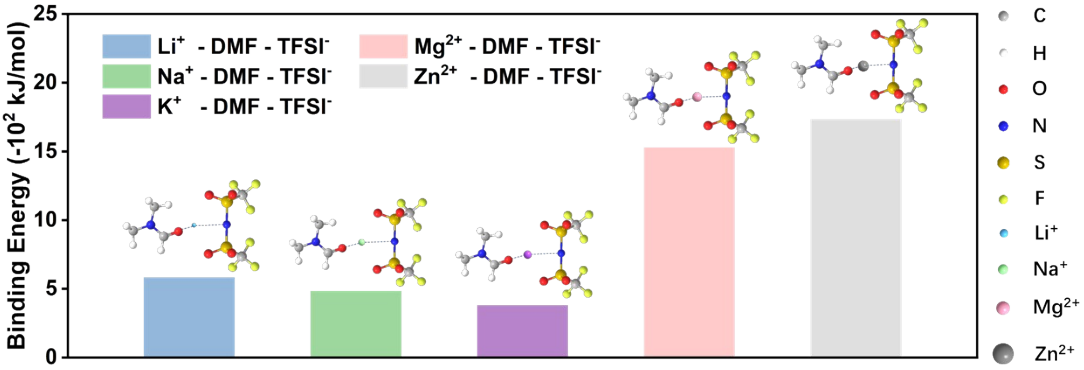

Figure S2. The binding energy of TFSI$^-$-Li$^+$-DMF, TFSI$^-$-Na$^+$-DMF, TFSI$^-$-K$^+$-DMF, TFSI$^-$-Mg^{2+}-DMF, and TFSI$^-$-Zn^{2+}-DMF.

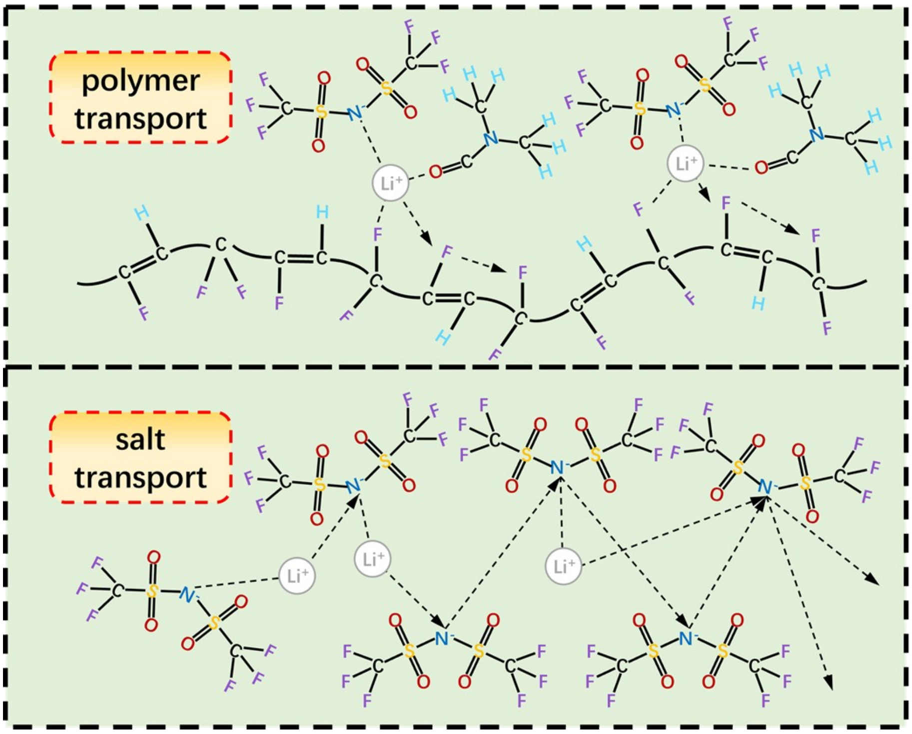

Figure S3. Schematic illustration for Li$^+$ transport along PVDF molecular chain (top) and Li$^+$ transport along TFSI$^-$ anionic cluster (bottom).

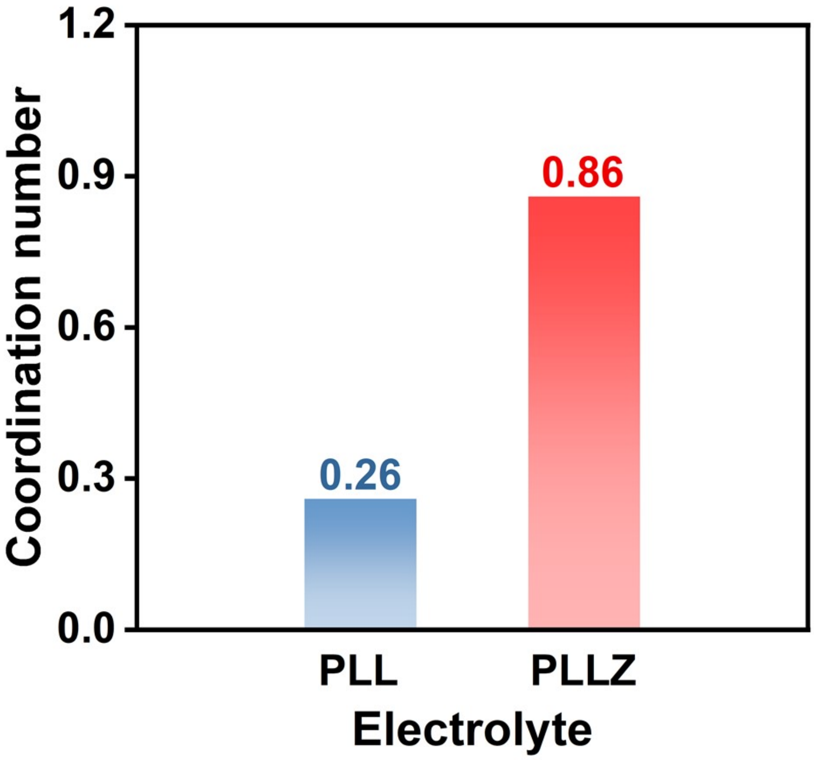

Figure S4. Coordination number of TFSI$^-$ in PLL and PLLZ electrolytes.

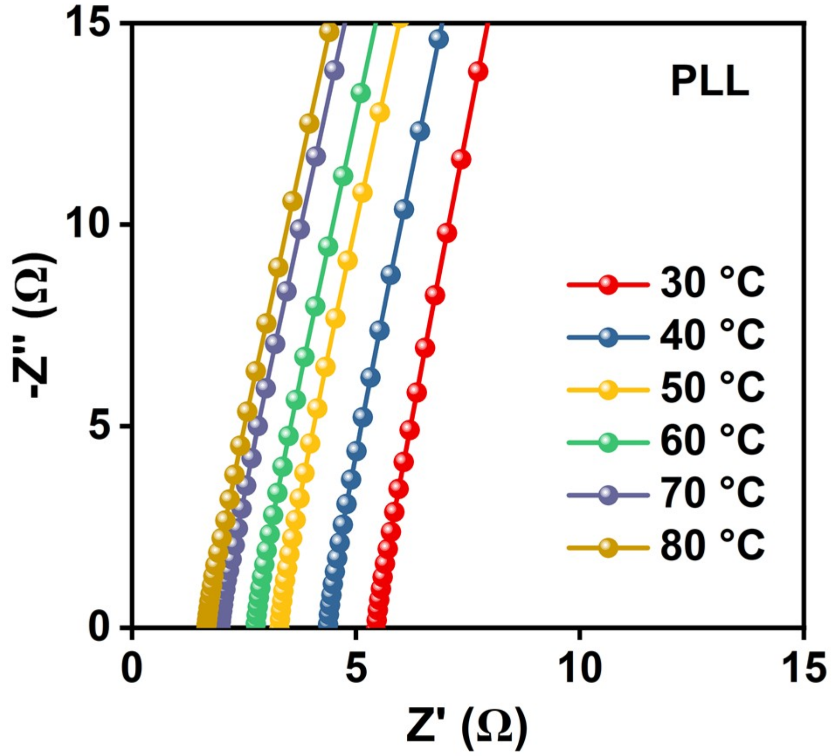

Figure S5. Impedance spectra of SS|PLL|SS cells in the temperature range from 30 to 80 ℃.

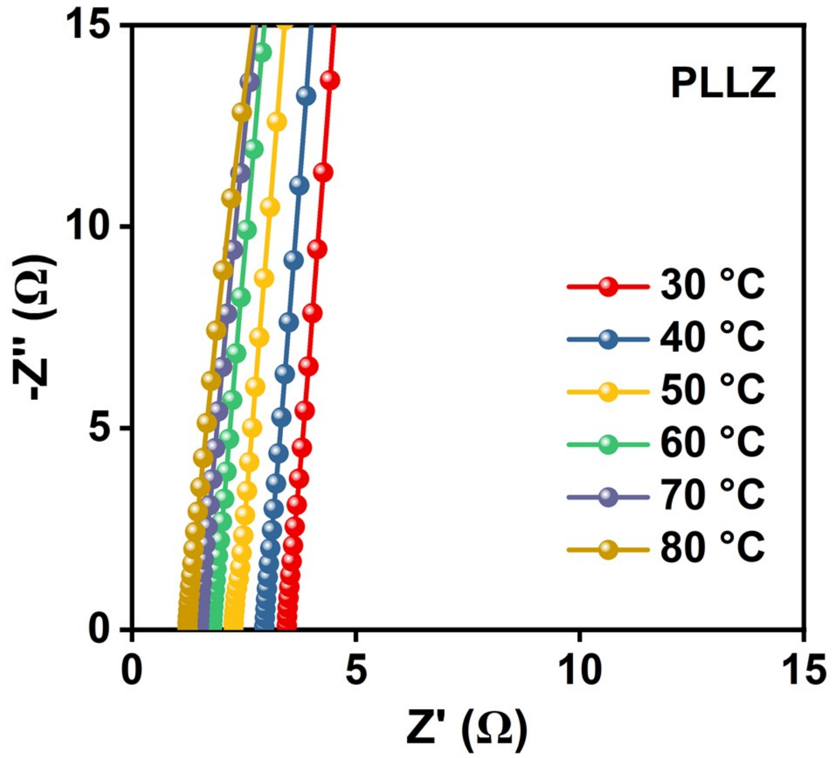

Figure S6. Impedance spectra of SS|PLLZ|SS cells in the temperature range from 30 to 80 ℃.

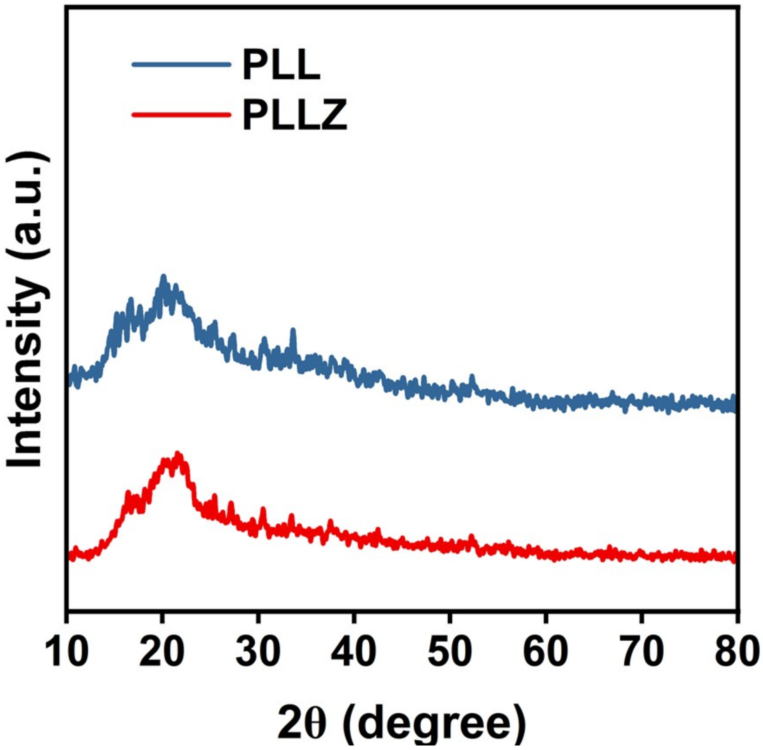

Figure S7. XRD patterns of PLL and PLLZ electrolytes.

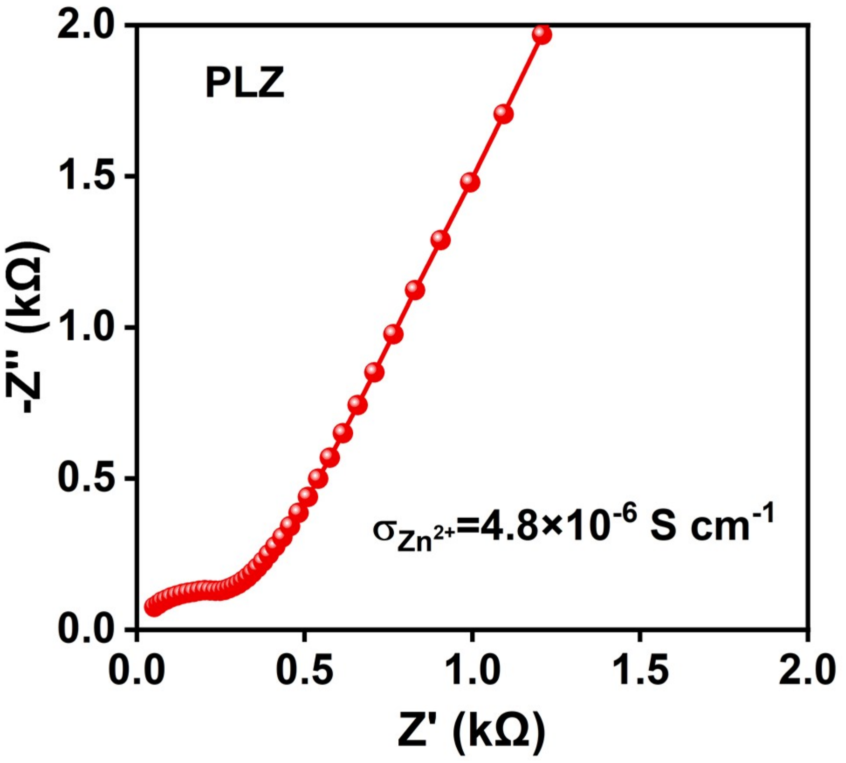

Figure S8. Impedance spectrum of SS|PLZ|SS cells at 30 ℃.

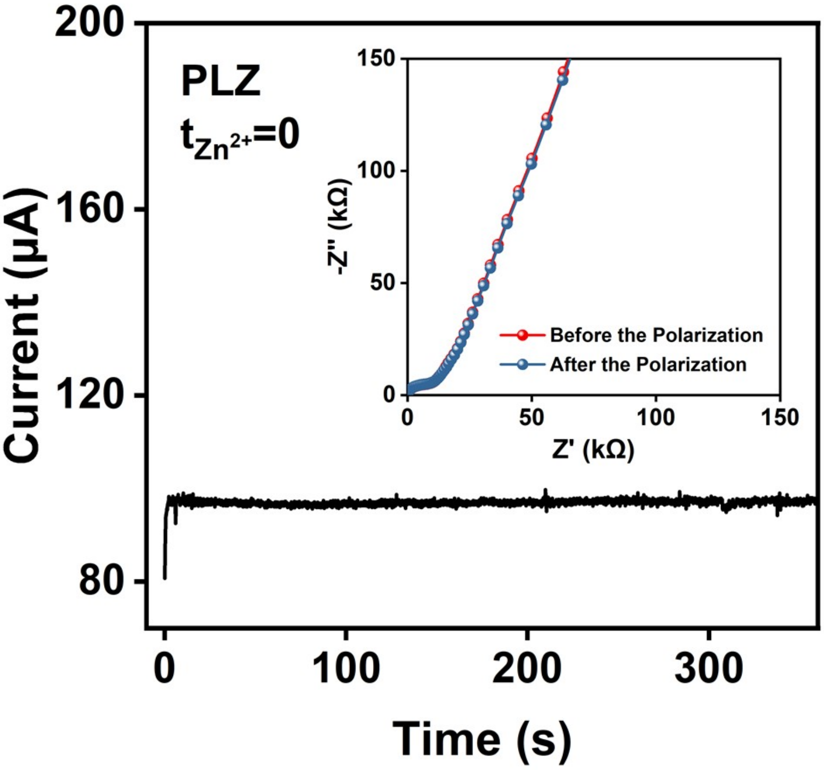

Figure S9. Chronoamperometry curves and Nyquist plots (inset) before and after the polarization of Li|PLZ|Li symmetric cells.

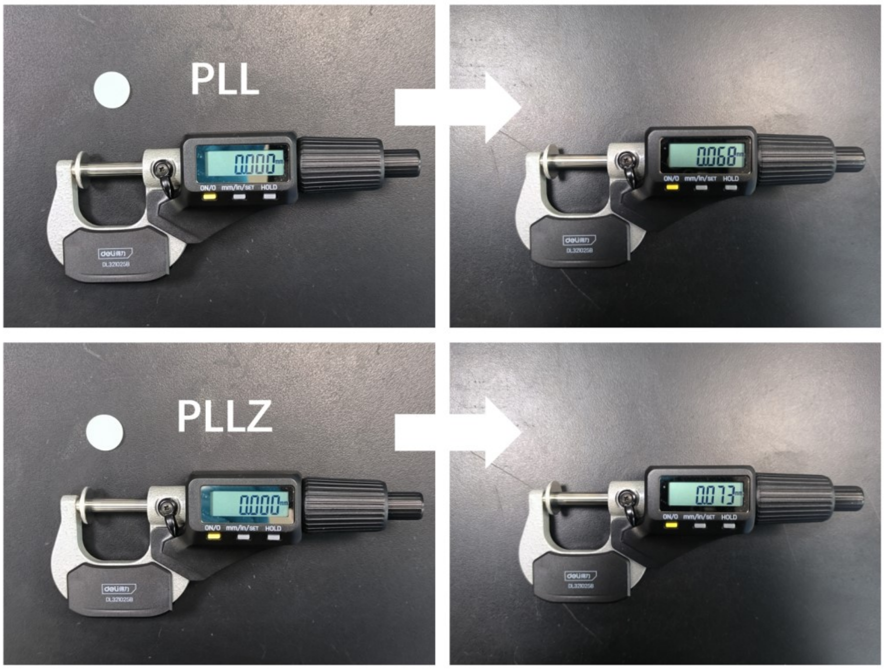

Figure S10. Digital photographs of PLL (top) and PLLZ (bottom) electrolytes.

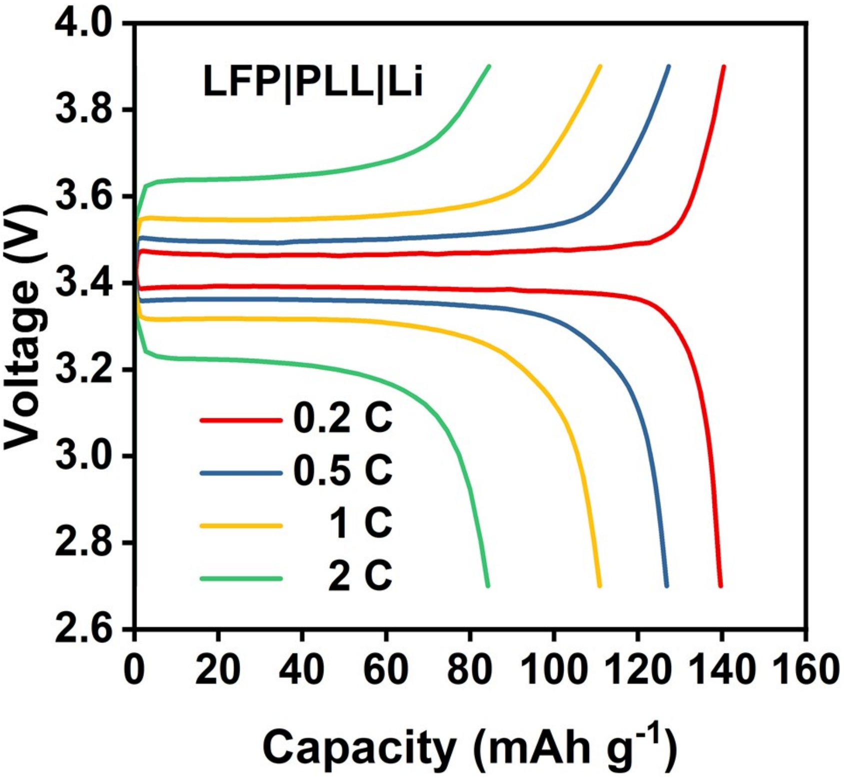

Figure S11. Charge/discharge profiles of Li|PLL|LFP cell at different rates.

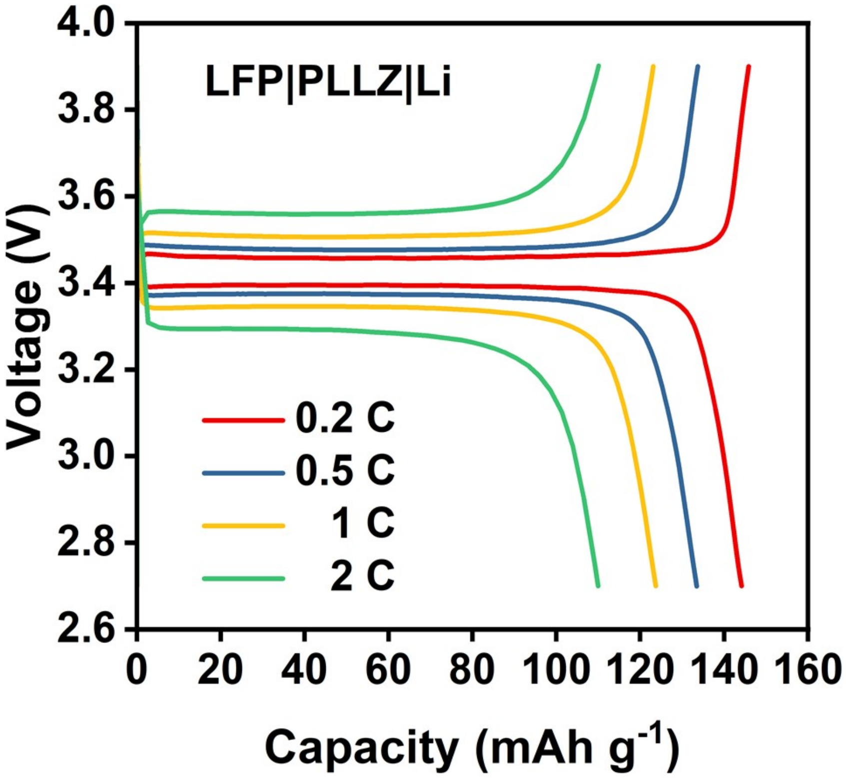

Figure S12. Charge/discharge profiles of Li|PLLZ|LFP cell at different rates.

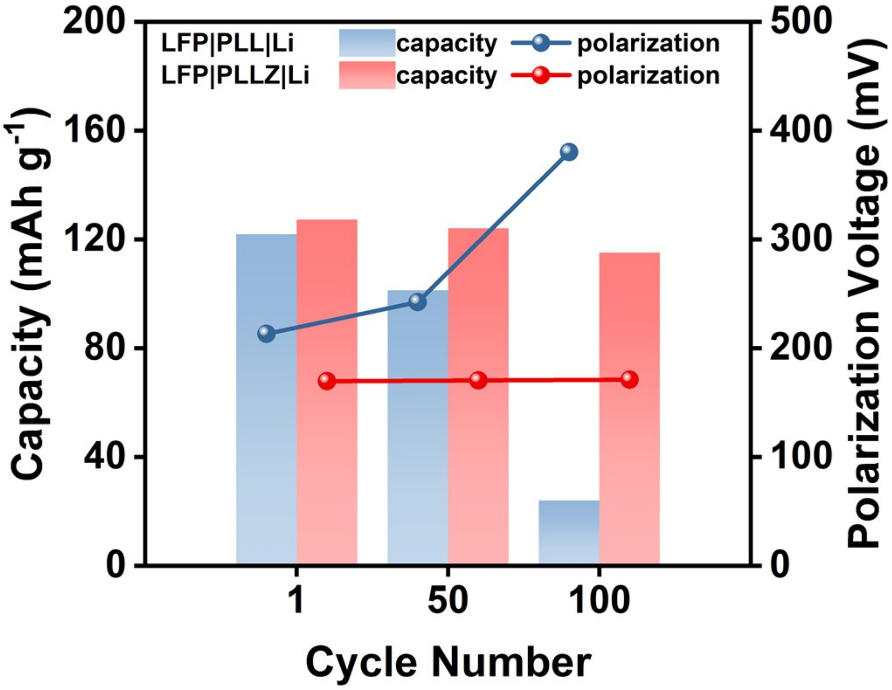

Figure S13. Capacity and polarization voltage of Li|PLL|LFP and Li|PLLZ|LFP cells during cycling.

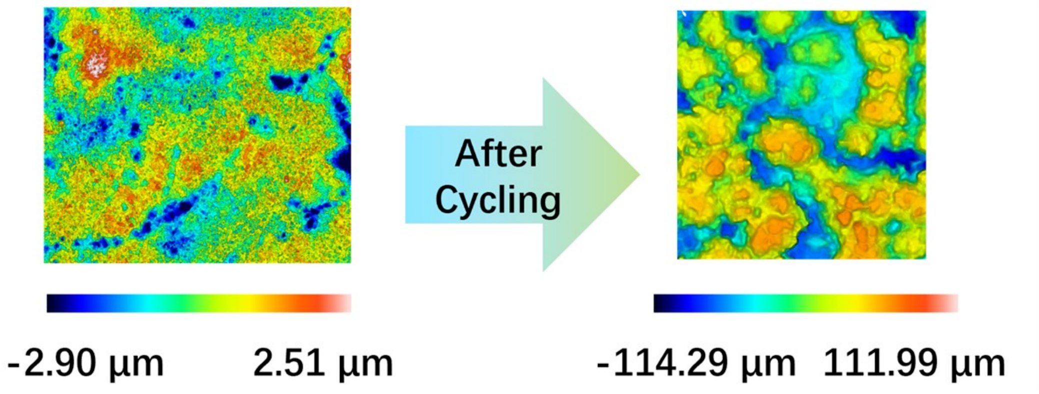

Figure S14. 2D optical profile images of PLL electrolyte before and after cycling in Li||Li symmetric cell.

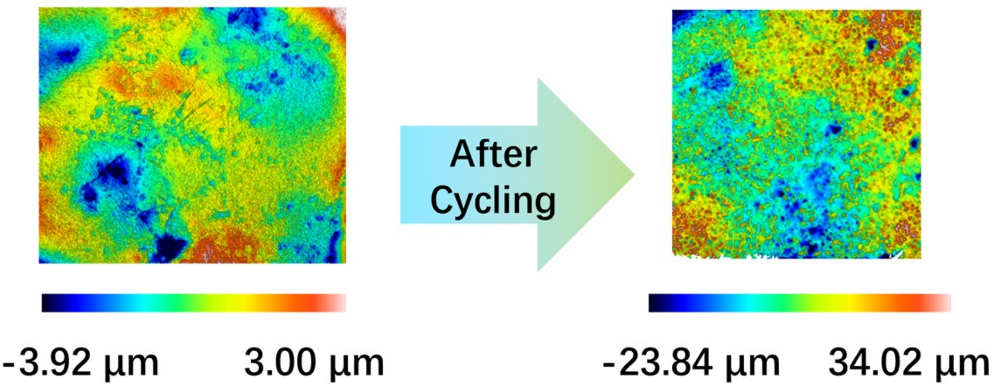

Figure S15. 2D optical profile images of PLLZ electrolyte before and after cycling in Li||Li symmetric cell.

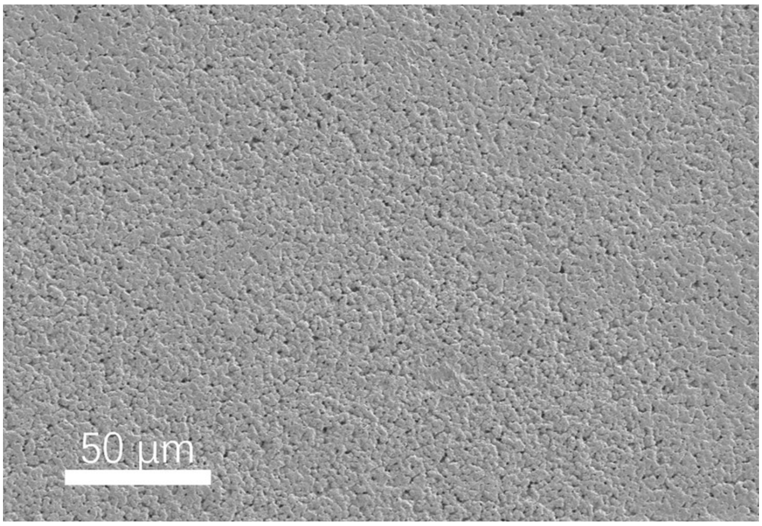

Figure S16. SEM image of PLL electrolyte before cycling.

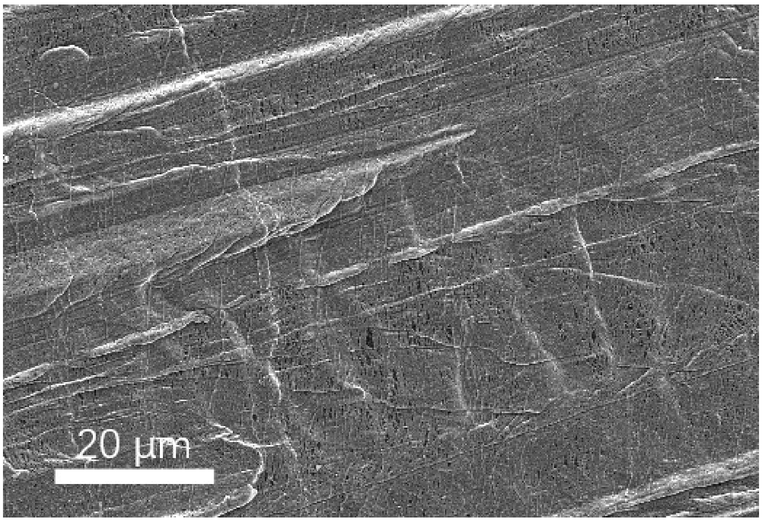

Figure S17. SEM image of fresh lithium metal.

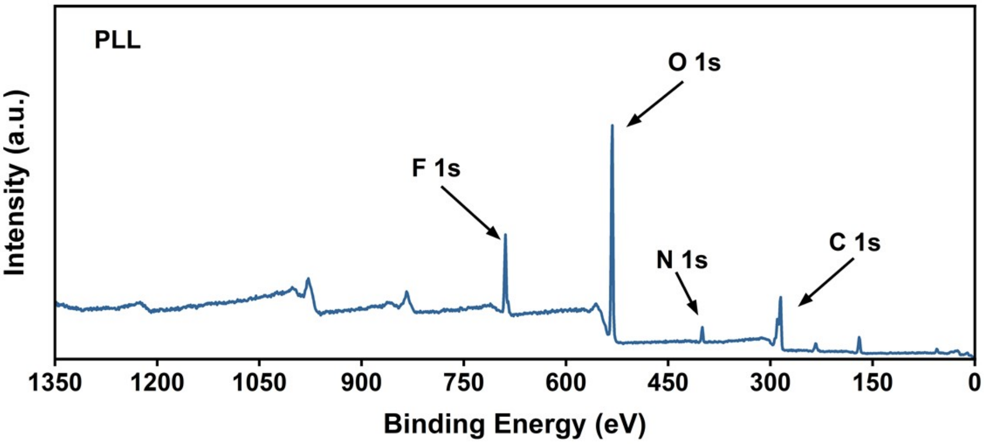

Figure S18. XPS spectrum of PLL-anode.

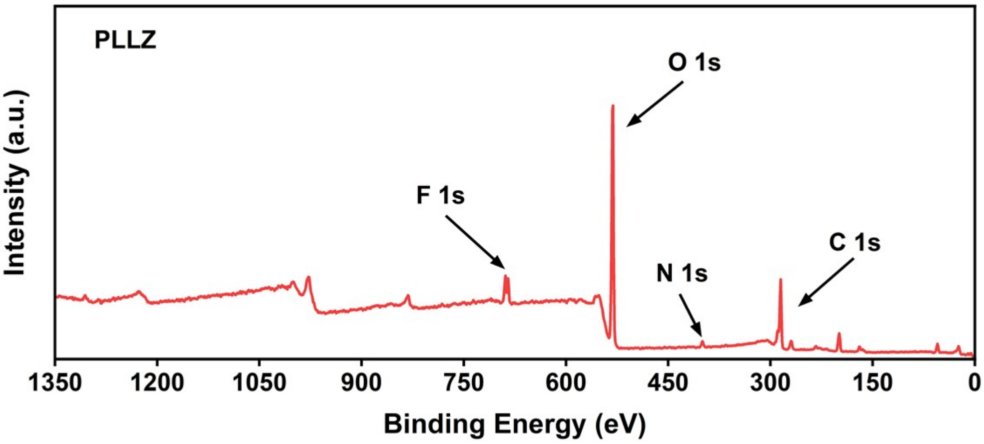

Figure S19. XPS spectrum of PLL-anode.

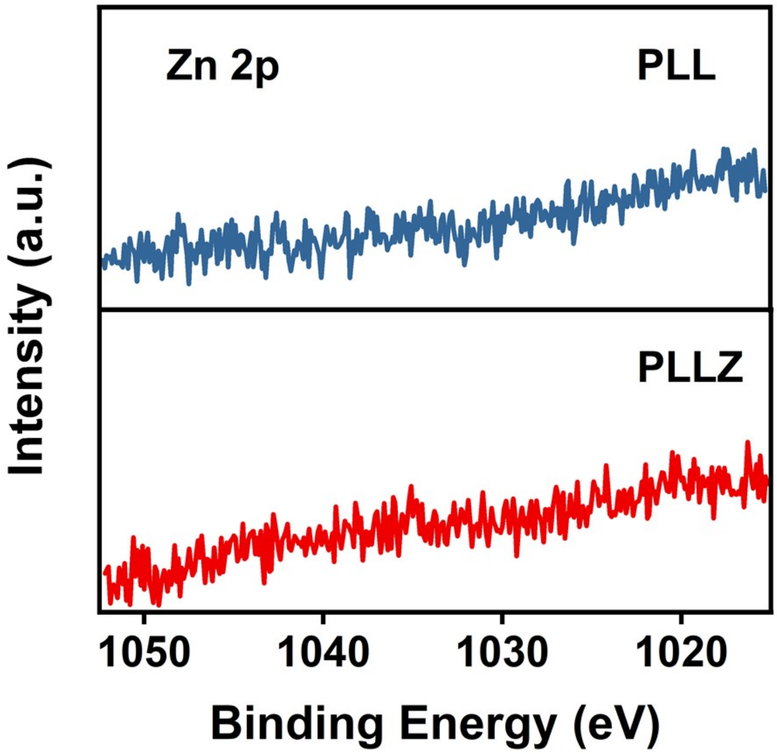

Figure S20. Zn 2p XPS spectra of PLL-anode (top) and PLLZ-anode (bottom).

Table S1. The binding energy of different coordination structures.

Type	Binding Energy (kJ/mol)
Li^+-DMF	-226.82
Na^+-DMF	-164.07
K^+-DMF	-119.99
Mg^{2+}-DMF	-583.71
Zn^{2+}-DMF	-706.27
$TFSI^-$-Li^+-DMF	-582.66
$TFSI^-$-Na^+-DMF	-483.80
$TFSI^-$-K^+-DMF	-381.00
$TFSI^-$-Mg^{2+}-DMF	-1527.98
$TFSI^-$-Zn^{2+}-DMF	-1734.82

Table S2. Coordination number of different coordination structures in PLL and PLLZ electrolytes.

Electrolyte	Pair	Distance (Å)	Coordination number
PLL	Li^+-$TFSI^-$	2.79	0.26
PLLZ	Li^+-$TFSI^-$	2.79	0.86
	Zn^{2+}-$TFSI^-$	3.01	0.34

Table S3. The ionic conductivities of PLL and PLLZ electrolytes in the temperature range from 30 to 80 ℃.

Temperature (℃)	Ion conductivity （mS cm^{-1}）	
	PLL	PLLZ
30	0.552	1.060
40	0.688	1.240
50	0.915	1.620
60	1.090	2.060
70	1.520	2.470
80	1.810	2.970

Table S4. Cycling performance of PVDF-based CPEs in Li||Li symmetric cells.

Electrolyte	Current Density (mA cm^{-2})	Time (h)	Ref.
PVDF/LiTFSI+Zn(TFSI)$_2$/LLZTO	**0.2**	**780**	**This work**
PVDF/LiDFOB/LLZTO	0.25	270	5
PVDF/LiTFSI/PCIL@LZSP	0.5	200	6
PVDF/LiFSI/h-PAN@MOF	0.5	500	7
PVDF-HFP/LiFSI/LLZTO	0.3	240	8
PVDF/LiFSI	0.2	300	9

References

1 C. Jiang, Q. Jia, M. Tang, K. Fan, Y. Chen, M. Sun, S. Xu, Y. Wu, C. Zhang, J. Ma, C. Wang and W. Hu, *Angew. Chem. Int. Ed. Engl.*, 2021, **60**, 10871-10879.

2 J. Ming, Z. Cao, W. Wahyudi, M. Li, P. Kumar, Y. Wu, J. Hwang, M. N. Hedhili, L. Cavallo, Y. Sun and L. Li, *Acs Energy Lett.*, 2018, **3**, 335-340.

3 W. Xia, R. A. Abdalrahman, L. M. F. Fiallos, A. M. B. Al-Dhalimy, P. S. Bains, A. H. Shather, U. K. Radi, A. Alawadi and Y. Elmasry, *Inorg. Chem. Commun.*, 2024, **161**, 112063.

4 E. E. Ushakova, A. V. Sergeev, A. Morzhukhin, F. S. Napolskiy, O. Kristavchuk, A. V. Chertovich, L. V. Yashina and D. M. Itkis, *Rsc Adv.*, 2020, **10**, 16118-16124.

5 M. Li, H. An, Y. Song, Q. Liu, J. Wang, H. Huo, S. Lou and J. Wang, *J. Am. Chem. Soc.*, 2023, **145**, 25632-25642.

6 L. Zhu, J. Chen, Y. Wang, W. Feng, Y. Zhu, S. F. H. Lambregts, Y. Wu, C. Yang, E. R. H. van Eck, L. Peng, A. P. M. Kentgens, W. Tang and Y. Xia, *J. Am. Chem. Soc.*, 2024, **146**, 6591-6603.

7 Y. Ma, Y. Qiu, K. Yang, S. Lv, Y. Li, X. An, G. Xiao, Z. Han, Y. Ma, L. Chen, D. Zhang, W. Lv, Y. Tian, T. Hou, M. Liu, Z. Zhou, F. Kang and Y. He, *Energy Environ. Sci.*, 2024, **17**, 8274-8283.

8 J. Zhang, Y. Zeng, Q. Li, Z. Tang, D. Sun, D. Huang, L. Zhao, Y. Tang and H. Wang, *Energy Storage Mater.*, 2023, **54**, 440-449.

9 X. Zhang, S. Wang, C. Xue, C. Xin, Y. Lin, Y. Shen, L. Li and C. W. Nan, *Adv. Mater.*, 2019, **31**, 1806082.